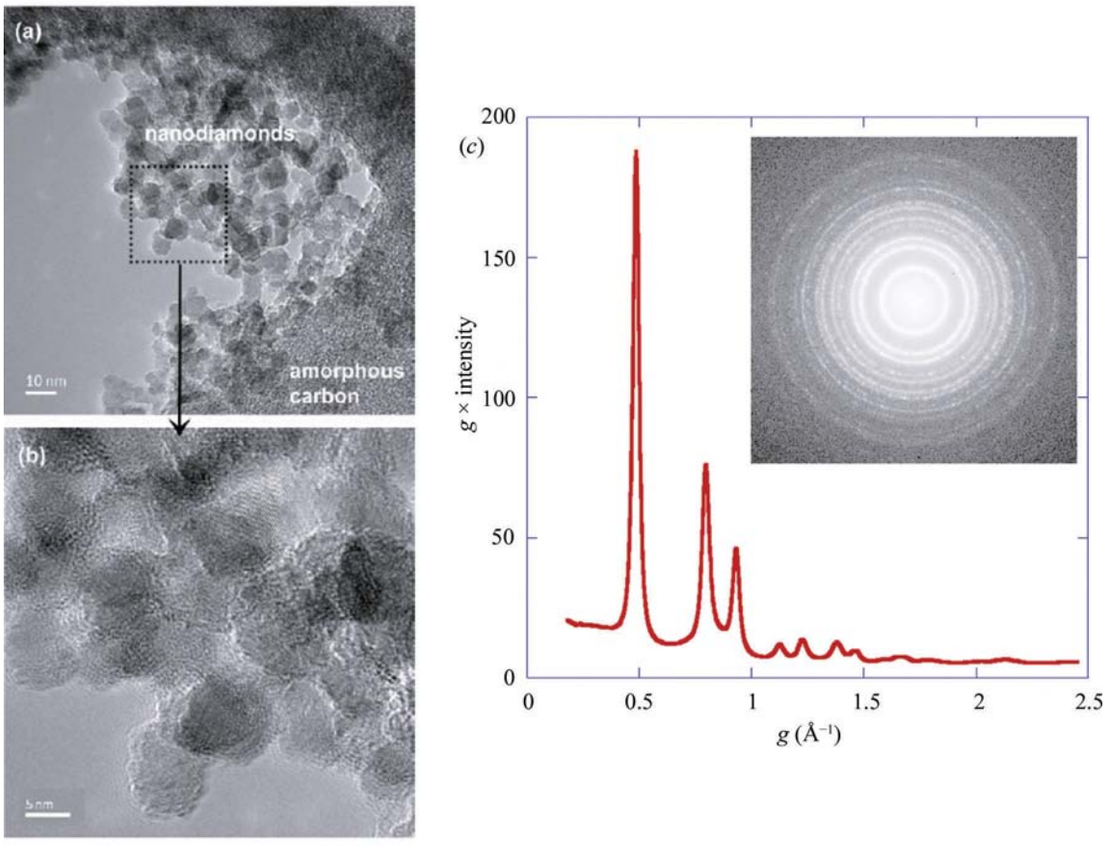

Figure 2.4.6
An example of electron powder diffraction recording for nanodiamonds. (*a*) A TEM image showing nanodiamond particles supported on amorphous carbon, (*b*) the magnified image from the boxed region of (*a*), and (*c*) the recorded electron powder diffraction pattern from nanodiamond particles and the obtained radial intensity profile.

fitting the diffraction ring position $R_d(\varphi)$ using a cosine expansion with

$$R_d(\varphi) = R + \sum_{n=1}^{N} \Delta R_n \cos n(\varphi - \varphi_n), \tag{2.4.16}$$

where R is the average radius (zero order) of the diffraction ring, ΔR represents the amplitude of distortion of order n and φ is the azimuthal angle. Once the distortion is calibrated and excluded from the data, the diffraction intensity integration can be simply carried out by summing the recorded diffraction intensity according to the radius using

$$I_n = \frac{1}{N} \sum I[i, j], \tag{2.4.17}$$

where the sum is taken over $R(i, j, i_0, j_0, \Delta R) \in \{n\delta, (n + 1)\delta\}$. Here the powder diffraction intensity is integrated in fine discrete steps along the radius of a diffraction pattern (corresponding to increasing scattering angle) with an interval of δ, the summation is done over all diffraction pixels that fall between the radius of $n\delta$ and $(n + 1)\delta$ and N is the number of these pixels.

Filtering the inelastic background is an option for electron microscopes equipped with an electron energy filter. A major contribution to the inelastic background in electron diffraction patterns comes from bulk plasmon excitation (Egerton, 2011). This can be filtered out by dispersing the electrons according to their energies using magnetic or electrostatic fields inside an electron energy filter and using a slit of a few eV in width around the elastic (zero-loss) electron beam. For use with an area electron detector for electron diffraction, the filter must also have a double focusing capability to function as an imaging lens. There are two types of electron imaging energy filters that are currently employed: one is the in-column Ω energy filter and the other is the post-column Gatan imaging filter (GIF). The in-column Ω filter is placed between the transmission electron microscope's intermediate and projector lenses and can be used in combination with IPs, as well as with a CCD or CMOS camera. The GIF is placed after the projector lens and the use of a GIF for electron diffraction typically requires the transmission electron microscope to be switched to a special low-camera-length setting. For electron diffraction, geometric distortions, isochromaticity and the angular acceptance are important characteristics of the imaging filter (Rose & Krahl, 1995). Geometrical distortions arise from the use of non-cylindrical lenses inside the energy filter. The distortion can be caused by optical misalignment, which is an issue with the GIF with its low camera-length setting. The amount of distortion can be measured using a standard calibration sample and corrected using numerical methods. Isochromaticity defines the range of electron energies for each detector position. Ideally, this should be the same across the whole detector area. The angular acceptance defines the maximum range of diffraction angles that can be recorded on the detector without a significant loss of isochromaticity (Rose & Krahl, 1995).

2.4.4. Phase identification and phase analysis

By J. L. Lábár

For known structures, powder diffraction patterns can be used for identification of the crystalline phases and quantification of their

volume fraction for samples containing multiple phases. These procedures are usually performed in two steps. First, the candidate phases must be selected to produce a shortlist of the structures that may be present in the sample. Preparation of the shortlist generally relies on *a priori* chemical information [obtained *e.g.* from energy-dispersive X-ray spectroscopy (EDS) or electron energy-loss spectrometry (EELS)] to reduce the number of candidate phases (crystalline structures) that are searched for (Lábár & Adamik, 2001; Lábár, 2006) in a comprehensive database such as the Powder Diffraction File (Faber & Fawcett, 2002). The identification of the crystalline phases in the experimental data is done through pattern fingerprinting. Final confirmation of phase identification is provided by the success of quantitative or semi-quantitative phase analysis, which determines the phase fractions and amount of texture.

In principle, the Le Bail structure-factor extraction (decomposition) method (see Chapter 3.5) could also be used for electron diffraction ring patterns from nanocrystals that are small enough to scatter kinematically or quasi-kinematically (Moeck & Fraundorf, 2007). The main advantage of this approach would be that no assumptions about the structure have to be made. However, none of the methods available for electron diffraction data follow this approach and identification of crystalline phases generally follows a different route [qualitative phase analysis (Lábár & Adamik, 2001) or traditional structural fingerprinting (Moeck & Rouvimov, 2010)].

After a two-dimensional ring pattern is integrated into a one-dimensional intensity distribution, the positions and intensities of peaks are extracted. The positions of the diffraction peaks are used as minimum information for fingerprinting. For successful phase identification the largest d values (at the smallest scattering angles) are crucial. Unfortunately, they are not always listed in the X-ray diffraction databases (Moeck & Fraundorf, 2007). Use of diffraction-peak intensities for fingerprinting has limited validity due to the deviation of electron diffraction intensities from the kinematic scattering formalism and the possible presence of texture in the sample. Phase analysis (fingerprinting) is complete when only one (set of) model structure(s) remains (out of several candidates listed in the previous step) on the basis of best fit between the model and the measured diffraction patterns. The addition of features to the Powder Diffraction File to make it more useful for phase identification using electron diffraction data is an active area of development.

Once a structural model is selected, the quantitative fit of diffraction intensities is performed. The quantitative modelling requires knowledge of the atomic positions within the unit cell. Atomic coordinates are not listed in the older PDF-2 database, but are given for many phases in the PDF-4+ database that combines five collections provided by different institutions. There are also open databases, like COD (http://www.crystallography.net/cod/), NIMS_MatNavi (http://crystdb.nims.go.jp/index_en.html) or AMCDS (http://rruff.geo.arizona.edu/AMS/periodictable.php). They also list atomic coordinates and can export structure data as CIF files.

For calculation of the electron structure factors, the electron atomic scattering factors are given in *International Tables for Crystallography*, Vol. C (2004). In the case of kinematical scattering, the intensity is proportional to the square of the electron structure factor F_{hkl}. If necessary, an absorption correction can be performed using the Weickenmeier & Kohl (1991) formalism.

Application of the quasi-kinematic formalism paves the way to giving an estimate of grain size in the beam direction (Lábár *et al.*, 2012). However, there is no straightforward correlation of this value with the actual crystal size or the thickness of the TEM sample. The grain size coming from the quasi-kinematic formula is also different from the size of the coherently scattering domains that could be determined from the broadening of the diffraction peaks (Ungár *et al.*, 2001), which is related to the lateral size of the crystallites (grains, particles) in the TEM sample.

In addition to peak positions and intensities, the peak shape and the background intensity have to be fitted. The pseudo-Voigt peak shape is most frequently used in electron diffraction phase analysis. The background intensity distribution in powder electron diffraction patterns is modelled empirically. The width of the diffraction peaks is an empirical parameter in the present implementation of phase analysis (Lábár, 2009). A Williamson–Hall type analysis of the variation of the experimentally observed peak width with the diffraction vector is also possible for simple profiles with well separated peaks (Gammer *et al.*, 2010); however, so far it has only been done for single-phase diffraction profiles with a known material without an attempt to combine it with phase analysis. Making the peak width dependent on grain size and defect structure (Ungár *et al.*, 2001) would in principle also be possible for phase analysis from powder electron diffraction data, but has not been implemented so far.

Selection of the appropriate structure model is done based on the value of the goodness-of-fit (GOF) criterion. For a one-dimensional electron diffraction profile recorded for n pixels, the GOF is given by

$$\mathrm{GOF} = \frac{1}{n-p}\sum_{k=n_0}^{n}\frac{1}{w_k}\left(I_k^{\mathrm{exp}} - I_k^{\mathrm{calc}}\right)^2, \tag{2.4.18}$$

where p is the number of parameters used in fitting, w_k is a relative weight of the intensity value at the kth pixel, and I_k^{exp} and I_k^{calc} are the experimentally measured and calculated intensity values for the kth pixel, respectively.

Structure models are described in parametric form (including experimental parameters, peak-shape parameters together with volume fractions of the phases and their fibre-textured components: p parameters altogether) and the p-dimensional parameter space is explored to calculate the GOF. The model with the smallest GOF is accepted. In phase analysis the best match is searched for by using the downhill simplex algorithm (Nelder & Mead, 1965). The semi-global simplex was found to be robust and allowed easy escape from local minima (Zuo & Spence, 1991) when used for fitting CBED patterns.

For polyphasic diffraction profiles, the volume fraction of phases is calculated at the end of the fitting procedure. It is assumed that the net diffraction intensity in each pixel is a linear combination of contributions of the individual phases (random and textured fractions are treated as independent model components). The over-determined set of equations is solved using least-squares minimization. The number of equations is reduced, while keeping the information content of all equations, by forming matrix $\mathbf{A}$ as

$$a_{i,j} = \sum_k \mathrm{Model}_k(i)\mathrm{Model}_k(j), \tag{2.4.19}$$

where summation is performed for all pixels k for the model functions of the ith and jth phases, and vector $\mathbf{b}$ as

$$b_i = \sum_k (\mathrm{Measured}_k - \mathrm{Background}_k)\mathrm{Model}_k(i). \tag{2.4.20}$$

The coefficients of the linear combination are obtained by solving for vector $\mathbf{x}$ the matrix equation $\mathbf{Ax} = \mathbf{b}$ using matrix inversion.

The coefficients of this linear combination $[x(i)]$ put the intensities of the peaks in phase i on the absolute scale. $I_{\max}(i)$, the intensity calculated on the absolute scale for the strongest (100%) diffraction peak of phase i, gives the intensity diffracted by one unit cell (structure factors are calculated for the atoms of one unit cell). Then $x(i)/I_{\max}(i)$ is the number of unit cells of phase i in the analysed volume. Consequently, the volume extended by phase i in the analysed volume is $V(i)x(i)/I_{\max}(i)$, where $V(i)$ is the volume of the unit cell of phase i. The volume fraction of phase f_i is then given by

$$f_i = \frac{V(i)x(i)}{I_{\max}(i)} \Big/ \sum_i \frac{V(i)x(i)}{I_{\max}(i)}. \qquad (2.4.21)$$

In addition to volume fractions of phases and their fibre-textured components, the same method can determine the variation (contraction, dilation, distortions) of the unit cell, provided experimental parameters specific to electron diffraction (*e.g.* the camera length and pattern distortion) are properly calibrated. The reliability of the camera-length calibration (systematic error) is usually around 2% (Williams & Carter, 2009); in the best cases accuracy of better than 0.3% has been reported (Lábár *et al.*, 2012). Consequently, only large variations in the lattice parameter can be determined reliably from powder electron diffraction data and the typical accuracy of powder X-ray diffraction cannot be attained.

There are two main advantages of phase analysis from powders by electron diffraction compared with X-ray diffraction. First, much smaller volumes can be studied. Diffraction information can be collected from thin layers of a few tens of nanometres thickness, enabling precise identification of the inspected volume. If needed, different lateral sections from different depths of a bulk sample can be studied by TEM, thus providing three-dimensional information about the sample. In a non-homogeneous sample, electron diffraction data can be collected from different areas, allowing detection of different phases or texture components at a spatial resolution and sensitivity superior to X-ray diffraction methods (Lábár *et al.*, 2012).

The accuracy of the phase-content identification in a mixture for the major components is around 10–15% (Lábár *et al.*, 2012). The detection limit depends on the scattering power of the component. A weakly scattering phase of Cr in a strongly scattering matrix of Ag could only be detected at the content of 2%, while the presence of 5% Ag in a relatively weakly scattering Ni matrix allowed full quantification of the two phases (Lábár *et al.*, 2012). Thus, generally 5% (by volume) is accepted as the detection limit for powder electron diffraction experiments.

2.4.5. Texture analysis

By J. L. Lábár

The orientation distribution in a polycrystalline (nanocrystalline) TEM sample (used for powder electron diffraction) can either be random or a large fraction of grains can favour a special direction, *i.e.* the sample is textured. The texture can originate from the non-spherical shape of the particles (as in sedimentation geology or drop-drying of a suspension of nanoparticles on a TEM grid) or from energetic and/or kinetic conditions during nucleation and growth of grains in the formation of polycrystalline thin films on a substrate or, alternatively, the texture can be a result of mechanical deformation (as in drawing wires or rolling sheets of metals). Although the distribution of the preferred orientations can be very different, a few general types are frequently observed.

In the simplest case only one preferred-orientation vector characterizes the sample and the orientations of the grains are distributed arbitrarily around that direction. This situation is called *fibre texture* (single-axis texture). The most typical representatives of this texture class are sedimentation platy particles on a flat surface where the preferred-orientation vector is normal to the flat face of the particles, or a drawn metal wire where the preferred-orientation vector is directed along the wire axis. Another texture type frequently observed in the sedimentation of rod-shaped particles is described by the preferred-orientation vector being confined within a plane, but being arbitrarily oriented within this plane. Rolling of metal sheets results in other, more complex, but well characterized texture types: 'copper-type', 'brass-type' and 'S-type' (Mecking, 1985).

There are different ways to handle texture with electron diffraction. One approach is to collect the orientation information from individual nanograins in an automated area scan and reconstruct pole figures and inverse pole figures on a medium-sized population of grains (Rauch *et al.*, 2008). In principle, this is a single-crystal method analysing the information from an assembly of crystals. The Russian crystallography group developed the theory of arcs in oblique texture and used such textured patterns in structure analysis (Vainshtein, 1964; Vainshtein & Zvyagin, 1992). The *TexPat* software (Oleynikov & Hovmoller, 2004) was designed and effectively applied to determining unit-cell parameters and refining structure from oblique textured electron diffraction patterns. Tang *et al.* (1996) developed a method to determine the axis of texture and distribution of directions around that axis. The March–Dollase model (Dollase, 1986) for the description of pole densities was adapted for electron diffraction and used for the simulation of ring patterns (Li, 2010); however, no attempt was made to determine the phase fractions or textured fractions automatically.

A simplified automatic treatment of texture was implemented in the *ProcessDiffraction* software (Lábár, 2008, 2009). Partial texture is approximated by a linear combination of an ideally sharp fibre texture and a random distribution of components. Both the textured and the random components are treated as separately determined volume fractions during quantitative phase analysis (see Section 2.4.4). The advantage of the method is that the determination of the textured fraction is combined with simultaneous handling of a quasi-kinematic scattering by the Blackman approximation, and these two effects, which both modify the relative intensities, are treated simultaneously on a unified platform.

The application of the most general method for determining texture from powder electron diffraction patterns is restricted to the thinnest samples where kinematic scattering holds (Gemmi, Voltolini *et al.*, 2011). The method consists of recording a set of powder electron diffraction patterns at defined tilt steps of the two-axis goniometer, covering a considerable part of the solid-angle range usually used for recording pole figures. Azimuthal sections are integrated separately in 10° steps. The resulting large three-dimensional data set is fed into a variant of the Rietveld method called *MAUD* (Lutterotti *et al.*, 1997), which has built-in scattering factors for electrons. The orientation density function (ODF) is determined from the measured data by discretization of the orientation space. For texture fitting the *EWIMV* algorithm is used (Lutterotti *et al.*, 2004), which can be applied with irregular pole figure coverage and includes smoothing methods based on a concept of the tube projection. Pole figures from the smoothed